Environ. Sci. Technol. **2002**, *36,* 1783−1790

An Absolute Calibration for Gas-Phase Hydroxyl Measurements

THOMAS M. HARD,*
LINDA A. GEORGE, AND
ROBERT J. O'BRIEN

Chemistry Department and Environmental Sciences and Resources Program, Portland State University, P.O. Box 751, Portland, Oregon 97207

We describe a new method of calibrating tropospheric hydroxyl (OH) instruments. Ozone−alkene mixtures produce steady-state OH radical concentrations. The steady state is governed by competition between OH production in the reaction of ozone with the alkene and OH removal by reactions with the alkene, ozone, and the reactor wall. In a flowtube reactor transporting an ozone−alkene mixture, the OH wall loss rate can be measured by varying the alkene concentration. Delivery of the reaction mixture to the sampling entry of an atmospheric OH measurement instrument provides an absolute calibration of the instrument's response to OH. The present precision of calibration is ±8% (1-σ), based on reproducibility over a wide range of ozone concentrations. The accuracy (±43%) is limited by uncertainties in kinetic rate coefficients and OH yield, which can be improved. The calibration requires no photon flux measurements or lamp-dependent absorption coefficients, which have inherent, variable, systematic uncertainties, and it has been tested in field experiments.

Absolute calibration of tropospheric OH measurement instruments is important in atmospheric chemistry, due to the central role of the reactions of the OH radical in the remote, rural, and urban troposphere (*1*). External calibration of instrument response during field measurements is essential to the accuracy of OH data for use in photochemical models (*2*).

Several absolute OH calibration methods have been employed and are summarized in Table 1. The disadvantages of the hydrocarbon-loss method (*5*−*10*) are the length of time (>1 h) required to perform the calibration and the bulky apparatus that must be moved in changing between ambient and calibration modes. The disadvantages of the 185 nm H_2O photolysis method (*11*−*19*) are the requirements for accurate determination of (a) photon flux distribution, (b) effective residence time in the photolysis zone, and (c) OH wall loss. Problems (a) and (b) are avoided by simultaneous measurement of O_3 production by O_2 photolysis (*20*−*24*). In the latter case, differences in O_2 and H_2O absorption coefficients and concentrations, and different detection sensitivities of O_3 and OH, require the use of calibrated 185 nm attenuators. The spectral output of 185 nm lamps varies with age and temperature, so absorption of lamp radiation by Schumann−Runge transitions of O_2 must also be measured (*25*−*28*). The presence of OH wall loss, and any differences in the radial regions of the flow sampled by the O_3 and OH instruments, must also be taken into account.

Here we describe an absolute calibration method that uses steady-state OH concentrations generated by a dilute ozone−alkene mixture in a flowtube. Single-point calibrations and the return to ambient measurements are achieved with minimal interruptions in the ambient data stream. The competition between OH production and removal gives a relatively uniform radial profile of [OH], compared with photolysis methods. This method needs no measurements of photon flux, effective residence time, or absorption coefficient of lamp radiation by O_2. The calibration procedure yields a direct measurement of the OH wall loss that has been experienced in the flowtube by that portion of the flow that is sampled by the OH instrument. The precision of the response measurement is ±8%, and the accuracy is dominated by uncertainties in published kinetic coefficients, which can be improved.

Principal Reactions. The OH production reaction is

$$O_3 + \textit{trans}\text{-2-butene} \rightarrow [C^*, C] \rightarrow \alpha_1 OH + \alpha_2 HO_2 + \Sigma\alpha_{Pi} P_i \quad (R1)$$

where C* and C are short-lived intermediates that rapidly reach steady state at a concentration too low to influence OH by reaction with either O_3 or OH. P_i represents any product other than OH and HO_2, and its possible roles are analyzed in the Supporting Information. α_1, α_2, and α_{Pi} are the respective yields of OH, HO_2, and P_i. The gas-phase OH removal reactions are

$$OH + \textit{trans}\text{-2-butene} \rightarrow \text{products} \quad (R2)$$

$$OH + O_3 \rightarrow HO_2 + O_2 \quad (R3)$$

$$OH + HO_2 \rightarrow H_2O + O_2 \quad (R4)$$

Our experiments are conducted in flowtubes, with OH lifetimes between 5 and 20 ms, limited by R2 and R3. The OH lifetime with respect to R4 is greater than the gas residence time in the flowtube, making R4 negligible. Secondary reactions that may also affect [OH] are addressed in the Supporting Information, where we show that they are negligible under our experimental conditions. The OH wall reaction is

$$OH + \text{wall} \rightarrow \text{loss} \quad (Rw)$$

whose rate coefficient k_w is measured in the experimental procedure.

Steady-State Model. The above production and removal reactions govern steady-state OH, given by

$$[OH] = k_1\alpha_1 [O_3][A]/(k_2[A] + k_3[O_3] + k_w) \quad (1)$$

where [A] = [*trans*-2-butene]. We define $K_{T2B} \equiv k_1\alpha_1/k_2$. As [A] becomes very large, [OH] approaches K_{T2B} [O_3]. At all alkene concentrations, the characteristic relaxation time for this system toward steady-state [OH] is

$$\tau = \{1 - \ln(\exp(1) - 1)\}/(k_2[A] + k_3[O_3] + k_w) \quad (2)$$

where the bracketed constant equals 0.459. The resulting [OH] is supplied to the instrument to be calibrated, yielding an OH signal and a background. The net signal is measured with a modulation cycle in which half the time is devoted to measurement of the background. The resulting net signal

* Corresponding author phone: (503)725-3881; fax: (503)725-9525; e-mail: hardt@pdx.edu.

10.1021/es015646l CCC: $22.00
Published on Web 03/12/2002

TABLE 1. Absolute Calibration Methods for Tropospheric OH Instruments

OH source	required external measurements	required constants	OH instrument	uncertainty (%)
laser photolysis of O_3	photon flux distribution, $[O_3]$, $[H_2O]$	O_3 UV absorption, $O(^1D)$ yield and rate coefficients	1-atm LIF[a]	10[b]
photochemical OH from HC + NO + hv in CSTR[c]	tracer loss by GC, residence time	tracer rate coefficient	FAGE[d]	36[e]
O_3 + ethene CSTR	tracer loss by GC, residence time	tracer rate coefficient	FAGE[f]	36[e]
H_2O photolysis at 185 nm	photon flux distribution, effective residence time, OH wall loss	H_2O UV absorption coefficient	FAGE,[g] SICIMS[i]	40,[h] 42−62[j]
H_2O photolysis at 185 nm	$[O_3]$, absorption of lamp radiation by O_2, OH wall loss.	H_2O UV absorption coefficient	FAGE[k]	40,[l] 30,[m] 23[n]
O_3 + alkene steady-state flow system	$[O_3]$, relative flow rate of alkene	K_{T2B}, or α_1, k_1, and k_2[o]	FAGE[p]	8,[q] 43[r]

[a] LIF = laser-induced fluorescence. [b] Precision only (*3, 4*). [c] CSTR = continuously stirred tank reactor. [d] FAGE = fluorescence assay with gas expansion or low-pressure LIF (*6−9*). [e] Accuracy (*10*). [f] Reference *10*. [g] References *11−15*. [h] Accuracy (*13−15*). [i] SICIMS = selected ion chemical ionization mass spectrometry (*16−19*). [j] Accuracy (*18, 19*). [k] References *20−24*. [l] Accuracy (*21*). [m] Accuracy (*22*). [n] Accuracy (*24*). [o] Defined in text. [p] This work. [q] Precision. [r] Accuracy.

rate, S_{OH}, in photons s^{-1} averaged over this cycle, is

$$S_{OH} = R[OH] \quad (3)$$

where R is the instrument response in photons s^{-1}/(molec cm^{-3}). Combining eqs 1 and 3

$$\frac{1}{S_{OH}} = \frac{1}{RK_{T2B}[O_3]} + \frac{1}{RK_{T2B}[O_3]}\left(\frac{k_w + k_3[O_3]}{k_2}\right)\frac{1}{[A]} \quad (4)$$

If we plot $1/S_{OH}$ vs $1/[A]$, eq 4 implies a linear graph with a slope $m = (k_w + k_3\,[O_3])/(k_2\,RK_{T2B}[O_3])$. The y-intercept, $b = 1/(RK_{T2B}[O_3])$, is the limiting value of $1/S_{OH}$ as the alkene concentration approaches infinity. The expression for b contains 2 uncertain quantities besides R. The expression for m contains the same 2 plus 3 more, introducing greater susceptibility to systematic error in the calculation of R from m than from b. Therefore we use the intercept b to measure the OH response

$$R = 1/(bK_{T2B}[O_3]) \quad (5)$$

The ratio of slope to intercept

$$m/b = (k_w + k_3[O_3])/k_2 \quad (6)$$

is independent of R. According to eq 6, a series of calibrations at different ozone concentrations, each yielding m and b as above, should yield a linear plot of k_2 (m/b) vs $[O_3]$, with a y-intercept k_w and a slope k_3.

Thus the plot of eq 4 gives a direct calibration of the instrument's OH response and a direct measurement of the OH wall loss rate in the external flowtube. k_w does not appear in eq 5, R does not appear in eq 6, gas flow rates do not appear in either equation, and R is insensitive to proportional errors in the alkene concentration. This OH calibration is absolute, though obviously it is sensitive to the accuracies of O_3 measurement, the extrapolation to the intercept using eq 4, and K_{T2B}. K_{T2B} may be obtained either from published values of α_1, k_1, and k_2 or from an additional calibration of the OH instrument by any independent method that yields an accurate value of R.

Experimental Section

Figure 1 shows the apparatus we used in OH calibration, including the OH FAGE instrument to be calibrated, an atmospheric-pressure flowtube, and auxiliary apparatus for the delivery and monitoring of reagents.

Flowtubes. We used two cylindrical external flowtubes in the course of these experiments. One was of synthetic fused silica, 10 mm inside diameter, uncoated, and the other was

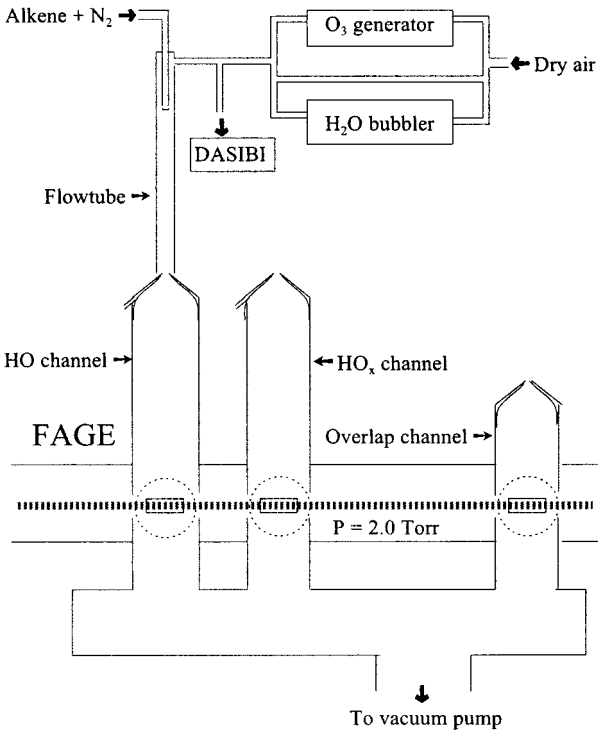

FIGURE 1. Schematic diagram of apparatus used in OH calibration experiments. In the flowtube, mixing of an alkene with O_3 generates steady-state OH. The outflow is sampled by a nozzle leading into the low-pressure FAGE instrument, where OH is detected by laser-excited fluorescence. Not shown are valves and mass-flow controllers in the reagent supply lines.

of stainless steel, 11.5 mm inside diameter, internally coated with halocarbon wax. Total flows were in excess of that required to supply one sampling nozzle of the OH instrument and ranged from 4.5 to 22 L/min. The resulting Reynolds numbers in the flowtubes ranged from 600 to 3000. The second, steel flowtube was part of an assembly that allowed rapid positioning over, and removal from, the ambient sampling nozzles during field measurements. The principal flow was of purified dry air (UPC grade), which we analyzed by gas chromatography, finding $CH_4 < 2$ ppm and no other hydrocarbon exceeding 1 ppb. At these levels, impurities yield negligible OH when mixed with ozone and negligible OH loss.

Ozone. Ozone was generated by UV photolysis of purified dry air and then diluted to final O_3 concentrations of 0.16−28 ppm (=μmol/mol). Ozone concentrations were measured with a Dasibi 1003AH ozone monitor, withdrawing a portion

TABLE 2. Rate Coefficients for the Ozone/*trans*-2-Butene System

	k(298 K), cm^3 $molec^{-1}$ s^{-1}	uncertainty (298 K) (%)	*k*(*T*), cm^3 $molec^{-1}$ s^{-1}
k_1	1.90×10^{-16} [a]	35[f]	$6.64 \times 10^{-15}\ e^{-1059/T}$ [a]
k_2	6.40×10^{-11} [b]	20[f]	$1.01 \times 10^{-11}\ e^{550/T}$ [b]
k_3	6.7×10^{-14} [c]	40[f]	$1.9 \times 10^{-12}\ e^{-1000/T}$ [c]
k_4	1.1×10^{-10} [c]	25[f]	$4.8 \times 10^{-11}\ e^{250/T}$ [c]
k_5	2.0×10^{-15} [c]	60[f]	$1.4 \times 10^{-14}\ e^{-600/T}$ [c]
k_w	27 s^{-1} [d]	20[g]	
	10−20 s^{-1} [e]		

[a] Reference *31*. [b] Reference *32*. [c] Reference *33*. [d] This work; limit as $[O_3] \rightarrow 0$. [e] Reference *34*, for Cl atoms in turbulent flow in 2.4 cm i.d. uncoated Pyrex. [f] Accuracy. [g] Precision.

TABLE 3. OH Yield of the Reaction of *trans*-2-Butene with Ozone

α_1	uncertainty
0.64 (at 760 Torr)[a]	factor 1.5[h]
0.24 (at 760 Torr)[b]	0.02[i]
0.69 (at 760 Torr)[c]	0.06[i]
0.65 (at 760 Torr)[d]	0.13[i]
0.54 (at 760 Torr)[e]	0.11[i]
0.61 (at 760 Torr, SF_6 0−70%)[f]	0.05[j]
0.62 (at 200 Torr)[f]	0.14[i]
0.59 (at 60 Torr)[f]	0.17[i]
0.4 (at 50 Torr)[g]	factor 1.5[h]
0.7 (at 2 Torr)[g]	factor 1.5[h]

[a] Reference *35*. [b] References *36* and *37*. [c] Reference *38*. [d] Orzechowska and Paulson, cited in ref *39*. [e] Reference *40*. [f] Reference *39*. [g] Reference *41*, corrected by factor 0.43 as suggested by ref *30*. [h] Accuracy. [i] Precision. [j] Standard deviation of 6 results.

of the total flow. For concentrations above 1 ppm, we corrected the Dasibi readings via Beer's law, following the manufacturer's recommendations. We also determined that the Dasibi O_3 scrubber removes at least 99% of O_3 at the 20 ppm level. The precision of the O_3 measurements is 0.001 ppm, and the accuracy is ±3%.

Alkene. *trans*-2-Butene (*E*-but-2-ene) was selected as the alkene for this study, based on its relatively high rates of reaction with O_3 and OH (Table 2) and several independent measurements of its OH yield (Table 3). *trans*-2-Butene (Matheson, 95%, impurities: *cis*-2-butene and other C4 hydrocarbons) was transferred to an evacuated cylinder, using a manometer to measure the pressure. The cylinder was then pressurized with dry N_2 to achieve a final *trans*-2-butene concentration of 18 ppm (±10%). This mixture, with added air to maintain constant total flow, was injected into the flowing O_3/H_2O/air mixture. In the fused-silica flowtube, we used a sliding coaxial injector with radially emitting ports 1 mm upstream from the sealed tip. Mixing was assisted by a wall-avoidance spacer, consisting of a bronze spring coil of oval longitudinal cross-section, immediately upstream from the ports. For the stainless steel flowtube, the *trans*-2-butene + air mixture was injected into the ozone + air flow in a 6 mm i.d. tubing tee, sufficiently far upstream from the flowtube to ensure adequate mixing. All flows were delivered by calibrated mass flow controllers. The OH calibration is flow-independent (provided the alkene flow controller is linear and any zero offset is subtracted from the flow reading). In most experiments the mean alkene concentrations in the flowtube ranged between 7×10^{11} and 2×10^{12} cm^{-3}.

OH Instrument. In our FAGE instrument,[10] a copper-vapor laser drove a Rhodamine 640 dye laser of our design,[9] whose tunable narrowband visible output was frequency-doubled to the UV region by a BBO crystal. In these experiments, the single-pass UV laser beam crossed three parallel low-pressure airflow channels: one for ambient OH, one for ambient $HO_x = OH + HO_2$, and one for a continuous source of higher-concentration OH ("overlap channel"). The latter was used to tune the laser to the Q_12 ($X^2\Pi$, v = 0; $A^2\Sigma^+$, v = 0) transition near 308 nm and to normalize the ambient signals to laser excitation power and spectral overlap with the OH transition. Since no windows separated the three flow channels, care was taken to prevent cross-flow from the overlap channel to the ambient channels, or from the HO_x channel to the OH channel, with diagnostic experiments verifying the absence of cross-flow. In each of the ambient sampling channels, air was continuously sampled by a nozzle, leading into a 48 mm i.d. cylindrical tube, 65 cm long, at a pressure of 2.0 Torr. During these experiments, nozzle entrance flows of either 4.5 or 11 L/min were used. After passing through the excitation cell, the channels joined in a manifold leading to a vacuum system (Edwards EH1200/DP180). Downstream from each ambient sampling nozzle, a carrier flow of 200 mL/min of dry air or N_2 was injected. Periodic addition of isobutane to the carrier flow removed 83% of external OH, enabling background subtraction (chemical modulation of the OH signal). In the HO_x channel (*5*, *8*, *10*, *29*), NO was injected continuously, to convert ambient HO_2 to OH for measurement, and the latter OH was likewise chemically modulated by addition of isobutane.

For diagnostic tests, we combined spectral modulation of the OH signal (by tuning the UV laser away from the OH absorption wavelength) with chemical modulation. Off-resonance excitation in the presence of isobutane gave the non-OH background. Subtraction of the non-OH background from the on-resonance signals, measured with and without isobutane, yielded the OH chemical modulation efficiency, a sensitive indicator of interferences. In another type of interference test, we attenuated the UV laser beam with a nondisplacing attenuator (consisting of a pair of counter-rotating fused-silica plates, adjusted for 2.5X attenuation). A third test involved substitution of perfluoropropene for isobutane as the modulating reagent.

Procedure. A typical full calibration for one channel used constant $[O_3]$, with OH signal measurements at a series of *trans*-2-butene concentrations. Diagnostic experiments with ozone in dry and moist air, and with the ozone−alkene mixture in dry and moist air and varying O_3 and total flow rate, were also performed. Air in the flowtube was within 2 °C of ambient temperature, which was measured in the vicinity of the flowtube during calibration.

Single-Point Calibrations. During field measurements of OH and HO_2, we calibrated the OH responses of the ambient OH and HO_x channels periodically. At night we performed full OH response calibrations using the above ozone−alkene method, requiring 20 min per channel. We also measured the HO_x channel's response to HO_x relative to OH, via 185 nm photolysis of an H_2O-air mixture in a synthetic-fused-silica flowtube. (Lacking a calibrated 185 nm radiometric system or a high-resolution vacuum-UV spectrometer to characterize the lamp spectrum relative to the Schumann−Runge bands of O_2, we did not attempt absolute OH calibration by photolytic methods.) During the day, we performed response calibrations of the OH channel at a single value of the *trans*-2-butene concentration. For the HO_x channel, the ozone−alkene flowtube system provided a reproducible HO_x reference signal. These single-point ("spot") calibrations were repeated at hourly or 2-hourly intervals during each day and evening.

Results

Response to OH. Figure 2 shows the results of three calibrations at constant injector position (30 cm) and constant total flow (6 L/min), using eq 4. Each calibration used a different O_3 concentration. In each calibration, we measured

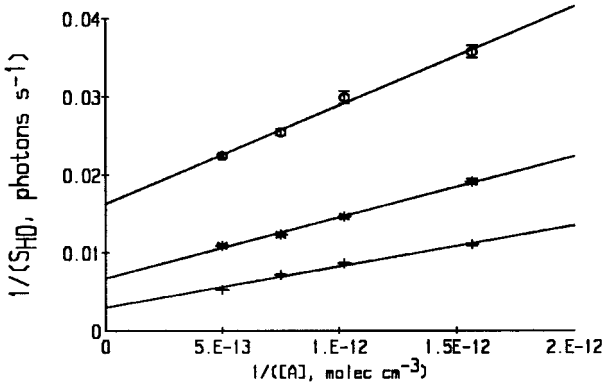

FIGURE 2. OH calibration by *trans*-2 butene ozonolysis, in a flowtube with mean residence time of 141 ms. Inverse OH signal vs inverse alkene concentration at three O_3 concentrations: ○, 5.5 ppm; *, 13.1 ppm; +, 27.6 ppm. Intercept gives response *R* (eqs 4 and 5). Error bars are ±1 standard error of the mean of sets of five or more measurements.

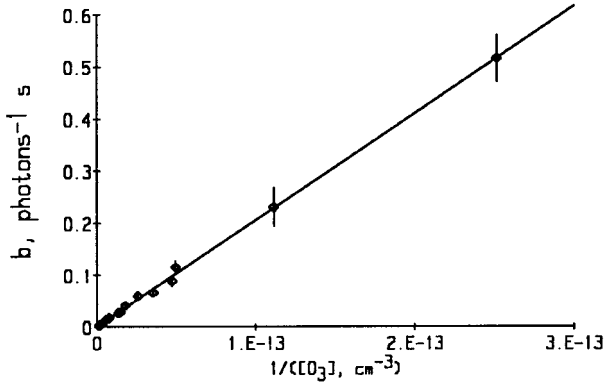

FIGURE 3. Dependence of *b*, the intercept of Figure 2, on $1/[O_3]$. *b* was measured in 17 calibration experiments similar to those in Figure 2, with O_3 ranging from 0.16 to 27.6 ppm. Each error bar is ±1 standard error of the fitted y-intercept of the corresponding experiment.

S_{OH} at four alkene concentrations, plotted $1/S_{OH}$ vs 1/[A], and performed a linear regression on the four experimental points, yielding the slope *m* and the intercept *b*.

Figure 3 shows the ozone dependence of the intercept *b* of the three fitted lines in Figure 2 and of 14 similar experiments covering an O_3 range from 0.16 to 27.6 ppm O_3 and an [OH] range from 5×10^6 to 8×10^8 molec cm^{-3}. The observed behavior of *b* agrees with that predicted by eq 4 and therefore allows the use of eq 5 to calculate the response *R* from an individual calibration experiment. Moreover, since $b = 1/(RK_{T2B}[O_3])$ (eq 4), the slope of the graph of Figure 3 is $m_2 = 1/(RK_{T2B})$. The measured slope is 2.05×10^{12} photon^{-1} s cm^{-3} (±1.0% standard error). Using K_{T2B} (298 K) = 1.87×10^{-6} (±47%), calculated from the published kinetic coefficients in Table 2 with $\alpha_1 = 0.63$, we find $R = 2.6 \times 10^{-7}$ s^{-1} $molec^{-1}$ cm^3.

Figure 4 shows that *R*, obtained via eq 5 in each of the 17 calibrations, is independent of $[O_3]$. Here we calculated K_{T2B} at the temperature measured in each experiment (298−305 K), obtaining an average $R = 2.4 \times 10^{-7}$. The relative standard deviation of the 17 measured responses in Figure 4 is 8%, and we take this as the precision of our measurement of *b* in an individual calibration by this method.

Wall Loss of OH. Figure 5 shows the ozone dependence of $k_2(m/b)$ obtained in the 17 calibrations. The intercept, $k_w = 27$ s^{-1}, is the wall loss rate coefficient in the absence of ozone. The slope, $(1.18 \pm 0.08) \times 10^{-13}$, is 1.77 times the literature value of k_3 (Table 2), exceeding the latter's

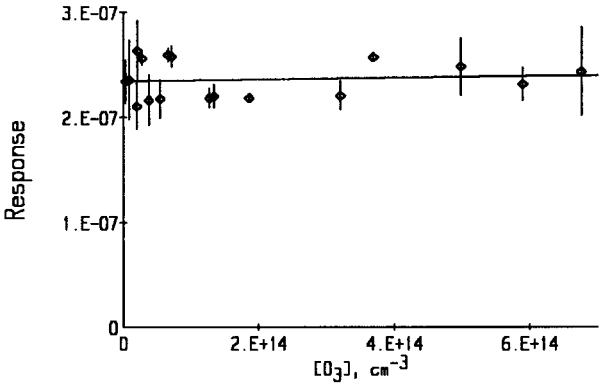

FIGURE 4. OH response *R*, in photons s^{-1}/(molec cm^{-3}), measured in a flowtube in the same 17 calibration experiments as Figure 3, using eq 5. Each error bar is derived from ±1 standard error of the fitted y-intercept of the corresponding experiment.

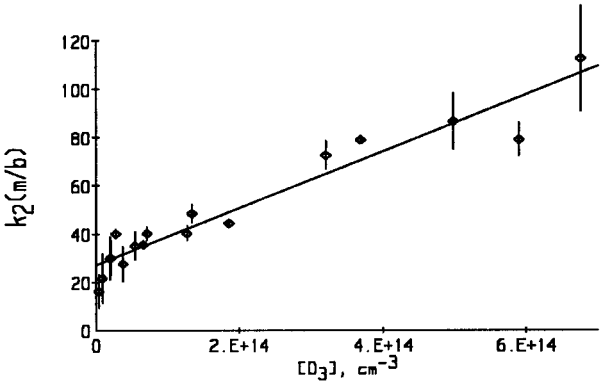

FIGURE 5. Dependence of $k_2(m/b)$ on ozone concentration in the same 17 calibration experiments as Figures 3 and 4. Each error bar is derived from ±1 standard error of the fitted slope of each experiment. Intercept is k_w (see eq 6).

uncertainty range. A possible explanation, gas-phase reaction of OH with other products of reactions R1 and R2, is discussed in the Supporting Information and found to be negligible for our experimental conditions. A reasonable explanation is an ozone-dependent contribution to the OH wall loss rate, though such a process has not been reported, to our knowledge, and may be worthy of further study. Inclusion of such processes in the kinetic model only adds terms to the numerator of the rightmost term of eq 4 and therefore does not influence the accurate measurement of *R*.

Variation of Injector Distance and Total Flow. Figure 6 shows results of calibration experiments at three injector positions. Here we multiplied $1/S_{HO}$ by $K_{T2B}[O_3]$ before plotting the data, to compensate for drift in $[O_3]$ between experiments, but the qualitative behavior of the graph is still that of eq 4. The y-intercept is nearly independent of distance, whereas the slope is 33% greater at the shortest distance. The mean flow time at this distance is 35 ms, while τ ranges from 3 to 6 ms; therefore the greater slope cannot be due to failure of the steady-state assumption for OH but may be ascribed either to incomplete mixing or to failure of the intermediates C and C* to reach local steady state. In any case, our routine OH calibrations are performed with flowtube residence times of 70 ms or longer, where the intercept is independent of injector distance.

Figure 7 shows results of calibrations at three total flow rates. The slopes at Re = 3000 (turbulent flow) and Re = 600 (laminar flow) are nearly equal, but the slope is 20% higher at Re = 2000 (indeterminate flow region), for which we have no explanation. The y-intercept, from which R is obtained,

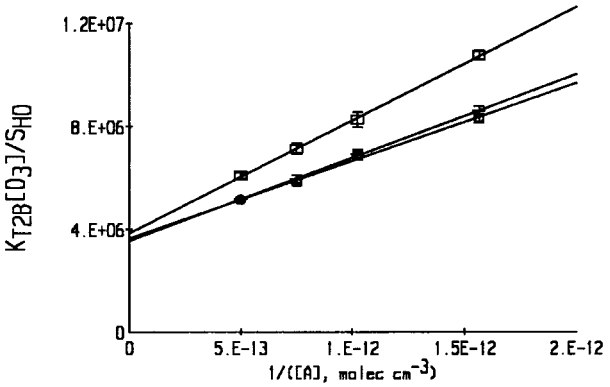

FIGURE 6. OH calibration by *trans*-2-butene ozonolysis, in a flowtube at approximately 10 ppm O_3. Inverse OH signal vs inverse alkene concentration, at injector-to-exit distances of 7.5 cm (□), 15 cm (+), and 30 cm (○). Error bars are ±1 standard error of the mean of sets of five or more measurements. Intercept gives response *R* (eqs 4 and 5).

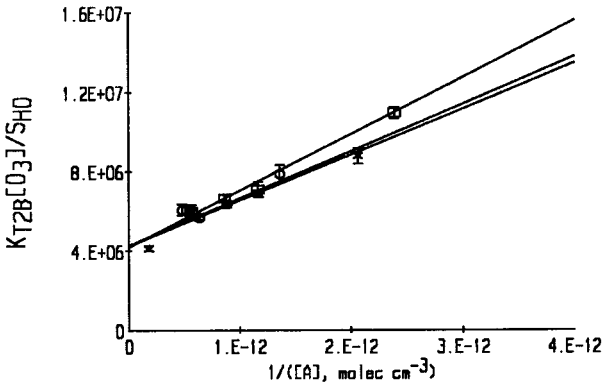

FIGURE 7. OH calibration by *trans*-2-butene ozonolysis. Inverse OH signal vs inverse alkene concentration, at total flow rates of 4.5 L/min (×, solid line, laminar flow), 14 L/min (□, dashed line, intermediate flow), and 22 L/min (○, solid line, turbulent flow). Error bars are ±1 standard error of the mean of sets of five or more measurements. Intercept gives response *R* (eqs 4 and 5).

is independent of flow rate and flow regime, demonstrating that the calibration is reproducible over a wide range of flow conditions.

Diagnostic Experiments. The above experiments were done in dry air. We performed additional experiments to evaluate possible interferences in FAGE. In experiments similar to those of Figure 2, calibration in moist air gave responses 5−10% lower than those in dry air. Tests in the absence of the UV laser beam found negligible chemiluminescence, due to the low duty cycle (<0.002 s/s) of the pulsed detection system. We measured the ozone interferences (due to reactions of laser-generated $O(^1D)$ with water vapor and with isobutane (*5*)) at the highest O_3 concentrations used, with no alkene present. The interferences were less than 2% of the calibrating signals obtained when both O_3 and *trans*-2-butene were present. These results are consistent with theoretical calculations using the model of Reference 5. The largest alkene concentration we used was too low to yield significant OH by $O(^1D)$ reaction.

Kroll et al. (*30*) observed photolytic interference in the laser-fluorescence detection of OH from the ozonolysis of terminal alkenes, which have lower OH yields than *trans*-2-butene. Reactions of $O(^1D)$, and photolysis of ozonolysis intermediates, were identified (*30*) as sources of this interference. To test for photolytic interference during calibration, we inserted a 2.5X attenuator in the UV laser beam. The attenuation resulted in no significant change in the normalized OH signal, in either dry or moist air, thus excluding photolytic interference in the calibration. With chemical modulation, photolytic OH is exposed to the modulating reagent for a very brief time, resulting in strong discrimination against this interference.

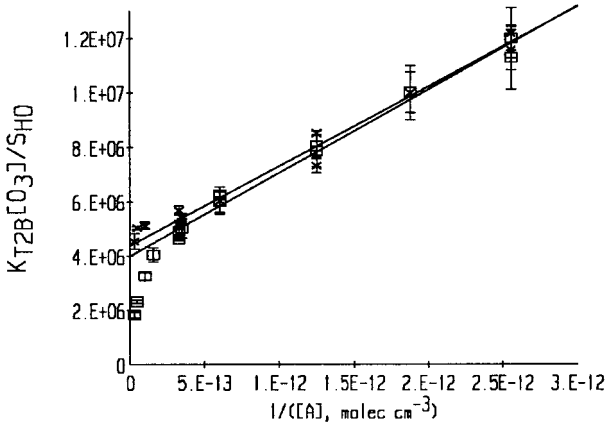

FIGURE 8. OH calibration using ozonolysis, with extended range of *trans*-2-butene concentrations (4×10^{11}−3.5×10^{13} cm^{-3}) in dry air (□) and in moist air at 1% H_2O (×). Points with alkene > 3×10^{12} cm^{-3} were excluded from linear fit.

We also explored *trans*-2-butene concentrations up to 12 times higher than those used in the experiments of Figures 2−6. The results are shown in Figure 8. In dry air, the observed OH signals in the high-alkene region deviated from the linear behavior obtained at lower alkene and were consistent with the presence of an additional OH source in the FAGE instrument, i.e., an interference. The evidence for a low-pressure interference (rather than a complication in the 1-atm system) is a reduction in the observed efficiency of chemical modulation from that obtained with OH from 185 nm H_2O photolysis. Repeated UV attenuation tests excluded laser photolysis as the cause of the interference. Moreover, substitution of perfluoropropene for isobutane as the modulating reagent gave no significant change in the signals or the chemical modulation efficiency. The alkene concentrations remained low enough to prevent significant direct production by Reaction R1 in the low-pressure instrument. However, we cannot exclude the possibility of an intermediate forming in the 1-atm flowtube, surviving transport through the FAGE nozzle and dissociating at low pressure to yield OH. Such OH would be modulated less efficiently than OH entering from the calibrator, due to reduced contact time with the modulating reagent.

In contrast, addition of ~1% H_2O to the flowtube mixture eliminated the above interference (Figure 8), yielding uniform linear behavior (in the sense of Figure 2 and eq 4) throughout the alkene concentration range as well as normal chemical modulation in the lower alkene range used for routine calibration. We used dry air in the survey experiments of Figures 2−7, done before we discovered the interference. The maximum alkene concentration in those experiments yielded negligible interference, with the likely exception of the leftmost measurement in Figure 7, at which the alkene was elevated by dilution in a smaller total flow. We used moist air for calibration of FAGE during OH field measurements.

We measured the OH signal at a radial displacement of the FAGE nozzle from the axis of the 1-atm flowtube by one-half the flowtube radius, relative to the on-axis OH signal, using the ozonolysis and photolysis OH sources. The nozzle inflow was half the flowtube outflow. With the ozonolysis OH source, the displacement decreased the signal by 12%, consistent with greater influence of OH wall loss near the wall. In contrast, with the photolysis OH source, the

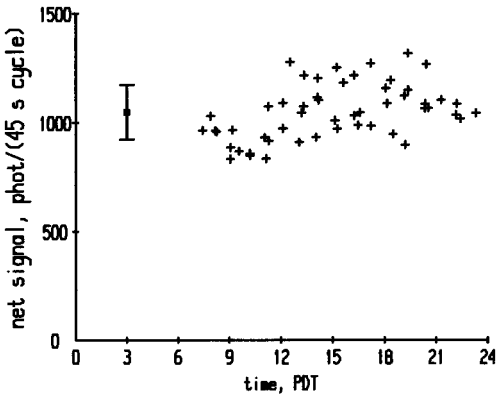

FIGURE 9. Reproducibility of OH spot calibrations of FAGE at Riverside CA, 9/19−22/1997, using *trans*-2 butene ozonolysis in a flowtube. +: calibrating signal, temperature-corrected. □: average, with ±1 standard deviation.

displacement increased the signal by a factor 2, consistent with longer residence time in the photolysis zone near the wall.

Comparison with Independent Calibrations. We also calibrated the FAGE instrument with a continuously stirred tank reactor (CSTR). In the latter method we measured OH via loss of 1,3,5-trimethylbenzene (*6, 8, 10*). To ensure a uniform spatial distribution of OH in the CSTR, we used an ozone−ethene mixture in moist air to generate OH, without NO or UV illumination (*10*). The response obtained with the ozone−ethene mixture was in good agreement with that obtained in the same chamber with UV illumination of an NO and 1,3,5-trimethylbenzene mixture (*10*). The CSTR ozone−ethene method yielded $R = 2.7 \times 10^{-7}$ photons s^{-1}/(molec cm^{-3}) (±36%). The differences between this value of R and those determined above from Figures 3 and 4 are less than the uncertainty of each calibration method.

In both calibration methods, the uncertainty is limited mainly by the accuracy of the published kinetic coefficients used in calculating R. Using the CSTR value for R, the present flowtube experiments (Figure 3), averaged over the 298−303 K temperature range, give an independent value of $K_{T2B} = 1.8 \times 10^{-6}$ (±37%) for *trans*-2-butene.

Field Reproducibility. Figure 9 shows results of OH "spot" calibrations during four consecutive days of our free-radical measurements at Riverside, CA, 9/19−9/22/1997. The data were obtained in moist air and are corrected for the temperature dependence of K_{T2B}. The standard deviation of the 52 results is 12% of the average, and there is an unexplained rising trend from morning to evening. The reproducibility of the "spot" results is comparable with that of HCAL (*10*), but with the advantage of direct relation to the absolute OH calibration.

Discussion

Time-Dependent Model. Accurate calibration depends on the validity of the steady-state OH expression in eq 1 for the flowtube experiments. To examine this validity, we used a time-dependent atmospheric chemistry model, based on the SAPRC-99 Fixed Parameter Mechanism (*42*), to which we have added OH wall loss and specific reactions for *trans*-2-butene. The model includes reactions R1−R5, reactions of observable products of R1, and a representative value of the measured OH wall loss rate. The model does not include reactions involving the important, but unobserved, intermediates of R1. Figure 10 shows the evolution of [OH] (and its controlling reaction rates) with time. The steady-state region is the plateau of constant OH at the center of the time range in Figure 10. The time constant τ for approach to this region is given in eq 2.

Two limits to the desired steady state are evident in Figure 10. First, at short residence times or low reagent concentrations, [OH] can fail to reach steady state at the flowtube exit. In this case, OH grows toward the plateau as $[OH] = [OH]_{ss}(1 - \exp(-t/\tau))$. In principle, data obtained with insufficient residence time can be corrected by dividing S_{HO} by $(1 - \exp(-t_{res}/\tau))$ before analysis by eqs 4−6. Since $1/\tau$ contains k_w, which is obtained by fitting the experimental data, this correction must be applied iteratively. However, in the present experiments, we employed conditions corresponding to the OH plateau region of Figure 10, where eq 4 is valid as written. Using the time-dependent model to simulate the worst case (the shortest injector distance in Figure 6) at the experimental alkene values, we found an error in the extrapolation to the intercept of only 1% relative to that calculated from the first term on the right of eq 4. The second limit to the plateau region is imposed by secondary reactions, of which we discuss five cases in the Supporting Information.

Low-Pressure Behavior. After gas expansion through the FAGE nozzle, too-high alkene concentrations can cause reactions R1 and R2 to persist at significant rates in the low-pressure region. The expansion decreases initial [OH], [O_3], and [*trans*-2-butene] by a factor of 380. Relative to [OH], the rates of gas-phase OH production and removal are decelerated by the same factor. Shifts in low-pressure steady-state [OH] would be expected from any pressure dependence of k_1, α_1, k_2, or k_3, and from differences in k_w between the external flowtube and the low-pressure probe. Therefore persistence of R1 and R2 in the low-pressure region can lead to miscalibration of the OH response. Moreover, chemical modulation (the addition of a reagent to remove OH and measure the background) can be defeated by the persistence of reaction R1 in the low-pressure region, resulting in a reduction in the apparent OH response. We avoid these errors by limiting the maximum alkene concentration, so that τ in the low-pressure region (> 1 s) is much longer than the mean transit time (≤0.04 s) between the nozzle and the excitation zone. This ensures that OH production by reaction R1 will not be significant after expansion. Then the calibrating OH reproduces the behavior of ambient OH in the instrument.

Direct OH Observation. Calvert et al.[31] note that OH production in ozone/alkene systems has been observed directly only at low pressures. The present experiments, using FAGE to detect OH in the ozone/*trans*-2-butene system, with reaction times in the 35−240 ms range, constitute direct observation of OH production at atmospheric pressure. This is discussed further in the Supporting Information.

Flowtube Model. The above discussion of the external flowtube is based on a plug-flow model, in which OH experiences a uniform wall loss rate regardless of its radial position in the tube. A more detailed model has the loss occurring only in the outermost cylindrical shell. In the presence of competition between R1 and R2, such a model predicts a relatively flat radial OH profile with a shallow maximum at the center. The calibration procedure directly measures the effective OH wall loss rate in the flowtube for that portion of the flow that is sampled by the OH instrument.

Uncertainties in Coefficients. As noted above, K_{T2B} can be obtained from published kinetic coefficients. Evaluations of the experimental kinetic studies of R1 and R2 give uncertainties at 298 K of 35% in k_1 and 20% in k_2 (Table 2). Under our chosen conditions, the coefficients k_3, k_4, and k_5 play no role in the measurement of R, so their relatively large uncertainties do not affect its accuracy.

Measurements of the OH yield α_1 (Table 3) are relatively recent and have not been evaluated in the literature. Atkinson and Aschmann (*35*) used cyclohexane to scavenge most of the OH produced in ozone/alkene systems and detected the

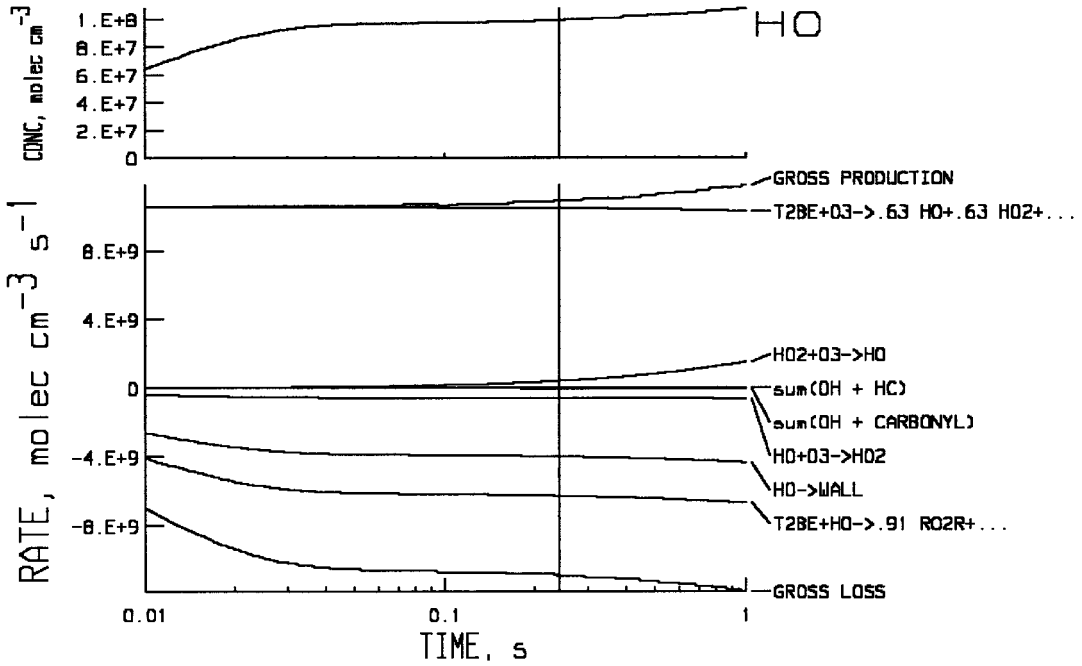

FIGURE 10. [OH], and its principal production and loss reaction rates, vs time. Model for flowtube at 0.041 ppm *trans*-2-butene, 3.5 ppm O_3, and $k_w = 40\ s^{-1}$. Rates with maxima below 1% of the maximum gross rate are omitted for clarity. Mean flowtube residence time is indicated by vertical line. Unlike OH, HO_2 grows with time, reaching 3×10^9 cm^{-3} at the mean residence time.

resulting products cyclohexanone and cyclohexanol. Four studies (*38*−*40*) (including Orzechowska and Paulson, cited in ref *39*) used a tracer method (*43*−*44*), in which the tracer, removed by OH and relatively unreactive to O_3, competes with the alkene for OH, and their relative disappearance rates are used to obtain α_1. These four studies, and Atkinson and Aschmann (*35*), agree within ±15% of their average, $\alpha_1 = 0.63$. We accept the latter average, with the ±15% range as its accuracy.

If K_{T2B} is calculated from published kinetic coefficients, then the present accuracies of α_1, k_1, and k_2 (±15%, ±35%, and ±20%) and of our O_3 measurements (±3%) contribute a systematic uncertainty of ±43% to the calibration. If instead K_{T2B} is calculated from the slope of Figure 3 with the value of R measured with the CSTR, then the systematic uncertainty in the flowtube steady-state OH calibration is reduced to ±37%. In either case, the random uncertainty of the calibration is the ±8% (1σ) precision of b, the intercept of eq 4.

The accuracies of α_1, k_1, and k_2 are subject to improvement by future measurements. Moreover, experiments to improve the accuracy of K_{T2B}, such as the one we report above, may be more productive than efforts on the individual coefficients. For example, K_{T2B} can be measured in laboratory experiments in which OH is generated by the ozone/alkene method and measured by its UV absorption at 308 nm. Spectral modulation is required to distinguish the OH absorption from the broader features of O_3, aldehydes, and other reaction products in this region. If UV absorption is the only OH measurement method used in the experiment, then the residence time of the reacting mixture in the absorption path must be kept short enough to avoid effects of reactions other than R1, R2, R3, and Rw, so that eq 1 is valid. In an alternative approach, secondary reactions are allowed, and the OH UV absorption in the ozone/alkene system is used to calibrate FAGE directly, as Stevens et al.[11] did with a photolytic OH source. In this approach, FAGE may then be used to measure K_{T2B} under different conditions in which secondary chemistry is excluded by design or by diagnosis.

Ozone−Alkene Intermediates. H_2O reacts with thermally stabilized carbonyl oxide intermediates that arise in ozone−alkene systems, altering the yields of stable products (*31*). Johnson et al. (*45*) found no effect of H_2O on the OH yield of the reaction of ozone with 2-methyl-2-butene. In the present work, using ozonolysis of *trans*-2-butene, we found that H_2O suppresses a low-pressure, nonphotolytic interference in the detection of OH. Since the interfering OH may arise from dissociation of an intermediate after passage through the FAGE nozzle, it is of interest for further investigation. Using alkene concentrations at which this interference is small, our results indicate no major effect of H_2O on the OH yield in the ozonolysis of *trans*-2-butene at atmospheric pressure.

Advantages and Disadvantages. The ozone/alkene reaction system provides laboratory or field OH instruments with an absolute, reproducible, precise, convenient, and automatable calibration, whose accuracy may be improved by additional work on kinetic rate coefficients.

The ozone/alkene OH calibration method is well-suited for FAGE. The necessary flows of air and reagents are easily delivered by a flowtube to the sampling nozzle, with a residence time sufficient to reach steady state at the flowtube exit. Within appropriate limits on the reagent concentrations, and the inclusion of H_2O vapor, the resulting OH behaves after expansion in the same way as ambient OH.

In contrast, this calibration method may not be suitable for any instrument in which OH is converted at atmospheric pressure to another species for detection. In such an instrument, the ozone/alkene steady-state system would regenerate OH with a characteristic time τ (eq 2) that is much shorter than that of OH in the ambient photochemical system. This deviation from ambient OH behavior would lead to a falsely high apparent OH response.

The present method has several advantages compared with the other field OH calibration methods in Table 1. With this method, no vacuum-UV flux radiometry is necessary, nor is there a need to account for variations in lamp spectral output with age and temperature. Ozone is easily and

accurately measured at the concentrations used. The steady state between reactions R1 and (R2 + R3) eliminates the influence of wall loss, makes that loss easy to measure, and improves the radial uniformity of OH.

Acknowledgments

This research was supported by EPA Grants R823319 and R826176 from the Science To Achieve Results (STAR) program of the National Center for Environmental Research. The results in this article have not been subjected to EPA review, so no official endorsement should be inferred.

Supporting Information Available

Discussions of secondary reactions, low-pressure interferences, variation of injector distance, OH yield coefficient, and direct OH observation. This material is available free of charge via the Internet at http://pubs.acs.org.

Literature Cited

(1) Crutzen, P. J.; Ramanathan, V. *Science* **2000**, *290*, 299−304.
(2) Crosley, D. R. *J. Geophys. Res.* **1997**, *102*, 6495.
(3) Davis, D. D.; Heaps, W. S.; Philen, D.; Rodgers, M.; McGee, T.; Nelson, A.; Moriarty, A. J. *Rev. Sci. Instr.* **1979**, *50*, 1505−1516.
(4) Rodgers, M. O.; Bradshaw, J. D.; Sandholm, S. T.; KeSheng, S.; Davis, D. D. *J. Geophys. Res.* **1985**, *90*, 12819−12834.
(5) Hard, T. M.; Chan, C. Y.; Mehrabzadeh, A. A.; O'Brien, R. J. *Environ. Sci. Technol.* **1984**, *18*, 768−777.
(6) Hard, T. M.; Chan, C. Y.; Mehrabzadeh, A. A.; Pan, W.; O'Brien, R. J. *Nature* **1986**, *322*, 617−620.
(7) Hard, T. M.; Chan, C. Y.; Mehrabzadeh, A. A.; O'Brien, R. J. *J. Geophys. Res.* **1992**, *97*, 9795−9817.
(8) Hard, T. M.; George, L. A.; O'Brien, R. J. *J. Atmos. Sci.* **1995**, *52*, 3354−3372.
(9) Chan, C. Y.; Hard, T. M.; Mehrabzadeh, A. A.; George, L. A.; O'Brien, R. J. *J. Geophys. Res.* **1990**, *95*, 18569−18576.
(10) George, L. A.; Hard, T. M.; O'Brien, R. J. *J. Geophys. Res.* **1999**, *104*, 11643−11655.
(11) Stevens, P. S.; Mather, J. H.; Brune, W. H. *J. Geophys. Res.* **1994**, *99*, 3543−3557.
(12) Mather, J. H.; Stevens, P. S.; Brune, W. H. *J. Geophys. Res.* **1996**, *102*, 6427−6436.
(13) Brune, W. H.; Faloona, I. C.; Tan, D.; Weinheimer, A. J.; Campos, T.; Ridley, B. A.; Vay, S. A.; Collins, J. E.; Sachse, G. W.; Jaeglé, L.; Jacob, D. J. *Geophys. Res. Lett.* **1998**, *25*, 1701−1704.
(14) Tan, D.; Faloona, I.; Brune, W. H.; Weinheimer, A.; Campos, T.; Ridley, B.; Vay, S.; Collins, J.; Sachse, G. *Geophys. Res. Lett.* **1998**, *25*, 1721−1724.
(15) Faloona, I.; Tan, D.; Brune, W. H.; Jaeglé, L.; Jacob, D. J.; Kondo, Y.; Koike, M.; Chatfield, R.; Pueschel, R.; Ferry, G.; Sachse, G.; Vay, S.; Anderson, B.; Hannon, J.; Fuelberg, H. *J. Geophys. Res.* **2000**, *105*, 3771−3783.
(16) Eisele, F. L.; Tanner, D. J.; Cantrell, C. A.; Calvert, J. G. *J. Geophys. Res.* **1996**, *101*, 14665−14679.
(17) Tanner, D. J.; Jefferson, A.; Eisele, F. L. *J. Geophys. Res.* **1997**, *102*, 6415−6425.
(18) Mauldin, R. L., III; Frost, G. J.; Chen, G.; Tanner, D. J.; Prevot, A. S. H.; Davis, D. D.; Eisele, F. L. *J. Geophys. Res.* **1998**, *103*, 16713−16729.
(19) Mauldin, R. L., III; Tanner, D. J.; Eisele, F. L. *J. Geophys. Res.* **1999**, *104*, 5817−5827.
(20) Aschmutat, U.; Hessling, M.; Holland, F.; Hofzumahaus, A. In *Physico-Chemical Behavior of Atmospheric Pollutants*; Angeletti, G., Restelli, G., Eds.; European Commission: Brussels, 1994; pp 811−816.
(21) Holland, F.; Hessling, M.; Hofzumahaus, A. *J. Atmos. Sci.* **1995**, *52*, 3393−3401.
(22) Creasey, D. J.; Halford-Maw, P. A.; Heard, D. E.; Pilling, M. J.; Whitaker, B. J. *J. Chem. Soc., Faraday Trans.* **1997**, *93*, 2907−2913.
(23) Kanaya, Y.; Sadanaga, Y.; Matsumoto, J.; Sharma, U.K.; Hirokawa, J.; Kajii, Y.; Akimoto, H. *Geophys. Res. Lett.* **1999**, *26*, 2179−2182.
(24) Kanaya, Y.; Sadanaga, Y.; Hirokawa, J.; Kajii, Y.; Akimoto, H. *J. Atmos. Chem.* **2001**, *38*, 73−110.
(25) Cantrell, C. A.; Zimmer, A.; Tyndall, G. S. *Geophys. Res. Lett.* **1997**, *24*, 2195−2198.
(26) Lanzendorf, E. J.; Hanisco, T. F.; Donahue, N. M.; Wennberg, P. O. *Geophys. Res. Lett.* **1997**, *24*, 3037−3038.
(27) Hofzumahaus A.; Brauers, T.; Aschmutat, U.; Brandenburger, U.; Dorn, H.-P.; Haussmann, M.; Hessling, M.; Holland, F.; Plass-Dülmer, C.; Sedlacek, M.; Weber, M.; Ehhalt, D. H. *Geophys. Res. Lett.* **1997**, *24*, 3039−3040.
(28) Creasey, D. J.; Heard, D. E.; Lee, J. D. *Geophys. Res. Lett.* **2000**, *27*, 1651−1654.
(29) Hard, T. M.; Chan, C. Y.; Mehrabzadeh, A. A.; O'Brien, R. J. *J. Geophys. Res.* **1992**, *97*, 9785−9794.
(30) Kroll, J. H.; Hanisco, T. F.; Donahue, N. M.; Demerjian, K. L.; Anderson, J. G. *Geophys. Res. Lett.* **2001**, *28*, 3863−3866.
(31) Calvert, J. G.; Atkinson, R.; Kerr, J. A.; Madronich, S.; Moortgat, G. K.; Wallington, T. J.; Yarwood, G. *The mechanisms of atmospheric oxidation of the alkenes*; Oxford University Press: New York, 2000.
(32) Atkinson, R. *J. Phys. Chem. Ref. Data: Monograph 1* **1989**.
(33) Atkinson, R.; Baulch, D. L.; Cox, R. A.; Hampson, R. F.; Kerr, J. A.; Rossi, M. J.; Troe, J. *J. Phys. Chem. Ref. Data* **1997**, *26*, 521−1011.
(34) Seeley, J. V.; Jayne, J. T.; Molina, M. J. *Int. J. Chem. Kinet.* **1993**, *25*, 571−594.
(35) Atkinson, R.; Aschmann, S. M. *Environ. Sci. Technol.* **1993**, *27*, 1357−1363.
(36) Gutbrod, R.; Meyer, S.; Rahman, M. M.; Schindler, R. A. *Int. J. Chem. Kinet.* **1997a**, *29*, 717−723.
(37) Gutbrod, R.; Kraka, E.; Schindler, R. N.; Cremer, D. *J. Am. Chem. Soc.* **1997b**, *119*, 7330−7342.
(38) Herman, P. P. Ph.D. Thesis, Portland State University, Portland, OR, 1997.
(39) Fenske, J. D.; Hassom, A. S.; Paulson, S. E.; Kawata, K. T.; Ho, A.; Houk, K. N. *J. Phys. Chem. A* **2000**, *104*, 7821−7833.
(40) McGill, C. D.; Rickard, A. R.; Johnson, D.; Marston, G. *Chemosphere* **1999**, *38*, 1205−1212.
(41) Kroll, J. J.; Clarke, J. S.; Donahue, N. M.; Anderson, J. G.; Demerjian, K. L. *J. Phys. Chem. A* **2001**, *105*, 1554−1560.
(42) Carter, W. P. L. *Documentation of the SAPRC-99 chemical mechanism for VOC reactivity assessment, Final Report to California Air Resources Board*; UC Riverside, 2000.
(43) Paulson, S. E.; Fenske, J. D.; Sen, A. D.; Callahan, T. W. *J. Phys. Chem. A* **1999**, *103*, 2050−2059.
(44) Rickard, A. R.; Johnson, D.; McGill, C. D.; Marston, G. *J. Phys. Chem. A* **1999**, *103*, 7656−7664.
(45) Johnson, D.; Lewin, A. G.; Marston, G. *J. Phys. Chem. A* **2001**, *105*, 2933−2935.

Received for review August 14, 2001. Revised manuscript received January 11, 2002. Accepted January 23, 2002.

ES015646L